FRIB ACCELERATOR BEAM DYNAMICS DESIGN AND CHALLENGES*

Q. Zhao#, A. Facco, F. Marti, E. Pozdeyev, M. Syphers, Y. Yamazaki, Y. Zhang, J. Wei, X.Wu,
FRIB/MSU, East Lansing, MI 48824, USA

Abstract

The Facility for Rare Isotope Beams (FRIB) will be a new national user facility for nuclear science and applications. This cw, high power, superconducting, heavy ion driver linac consists of a front end to provide various highly charged ions at 0.5 MeV/u, three superconducting acceleration segments connected by two 180° bending systems to achieve a final output beam energy of beyond 200 MeV/u for all varieties of stable ions, and a beam delivery system to transport multi-charge-state beams to a fragmentation target at beam power of up to 400 kW. The linac has an 80.5 MHz base frequency and utilizes four types of low-beta resonators with one frequency transition to 322 MHz after the first segment at beam energy of up to 20 MeV/u, where ion charge states are increased through a stripper. The challenges of beam dynamics design include the simultaneous acceleration of multi-charge-state ion beams to meet beam-on-target requirements, efficient acceleration of high intensity, low energy heavy ion beams, limitation of uncontrolled beam loss to less than 1 W/m, accommodation of multiple charge stripping scenarios, and other characteristic features. We report the recent optimizations on linac lattice, present the results of end-to-end beam dynamics simulations with machine errors, and discuss the simulation of beam tuning and fault conditions.

INTRODUCTION

The Facility for Rare Isotope Beams (FRIB), baselined as a 7-year, US$680 million construction project, is to be built at Michigan State University under a Cooperative Agreement with the US Department of Energy (DOE) [1]. High availability, maintainability, reliability, tunability, and upgradability are especially required for the FRIB accelerator to operate as a national scientific user facility. Since it received CD-1 (Approve Alternative Selection and Cost Range) from the DOE in September 2010, the facility has achieved a fully developed design capable of producing up to 400 kW of average beam power with energies beyond 200 MeV/u for all stable ion species, and delivering to the final target station a spot size and energy spread consistent with experimental requirements. The project is prepared to establish the performance baseline and the start of conventional facility construction. Space is reserved for potential future enhancements, such as energy upgrades, ISOL targets, and a light ion injector.

The FRIB driver linac is a cw heavy ion machine with high beam power (up to 400 kW). This machine has its unique features compared with high power proton ones. In contrast to high intensity spallation neutron sources and neutrino sources that require pulsed beams, most FRIB experiments will prefer cw beams. By choosing cw acceleration, a low peak beam current (average of < 1 emA) can meet the final beam power of 400 kW. Therefore, the space charge effects are mostly negligible except for the ion source and low energy beam transport. To maximize heavy ion beam intensity on the target, multiple charge states are accelerated simultaneously (e.g. 2 charge states of U^{33+} and U^{33+} before stripping, and 5 charge states of U^{76+} to U^{80+} after stripping). The acceleration of heavy ions is much slower than that of protons due to the low charge-to-mass ratio. But it is feasible to accelerate heavy ions from very low energy (0.5 MeV/u) with low-beta superconducting cavities and focusing solenoids housed in a cryomodule. Two-gap quarter- and half-wave resonators are chosen throughout the entire linac for efficient acceleration. The phase and amplitude of each cavity are independently adjustable, which makes it very flexible and efficient to accelerate varieties of ions with different charge-to-mass ratios. Heavy ions have much larger stopping powers (higher Bragg peaks) than protons, therefore, heavy ion beam losses result in higher power-density in material and tend to damage the surface of beam elements (e.g., niobium cavity) easily. The apertures of the FRIB accelerating

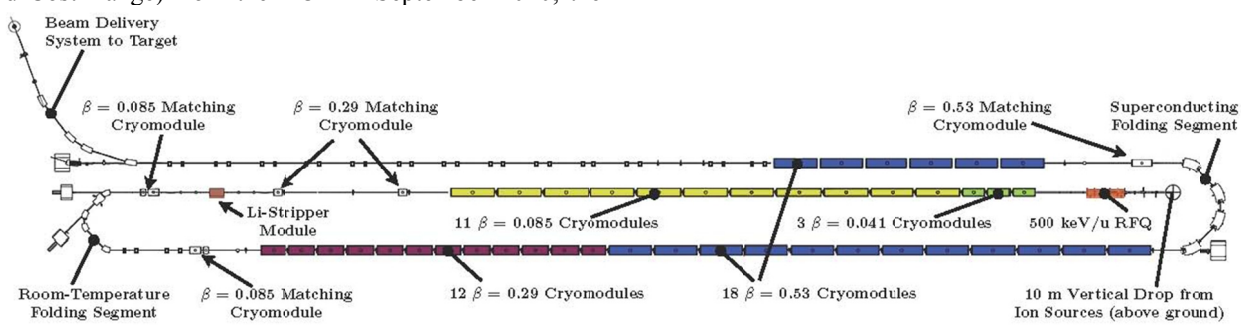

Figure 1: Layout of the FRIB accelerator at tunnel level (above-grade portion of the Front End not shown).

* Work supported by the U.S. Department of Energy Office of Science under Cooperative Agreement DE-SC0000661
# zhao@frib.msu.edu

ISBN 978-3-95450-118-2

structures are relatively small and the beam envelope reaches maxima in the cold solenoid locations inside cryomodules, while proton superconducting machines like the Spallation Neutron Source linac at ORNL use elliptical cavities with much larger apertures and their beam envelopes reaching maxima in the warm locations of the focusing quadrupole magnets. On the other hand, the radiation yields from heavy ions are much lower than those of protons with the same beam loss at similar beam energy. Although radiation shielding can be reduced, it is difficult to detect the losses of low-energy heavy-ion beams. Since conventional BLMs are not applicable at low beam energy, loss detection based on beam scraping is proposed for heavy ions.

ACCELERATOR LAYOUT OVERVIEW

The FRIB accelerator consists of a Front End, three superconducting acceleration segments (Segment 1, 2 & 3), which are connected by two 180° bending systems, and a Beam Delivery System, as shown in Fig. 1.

Over the past 2 years, many iterations of lattice design have been performed to optimize performance, reduce cost, and minimize risk. The linac was shifted northward by ~11 m while keeping the target position fixed to allow open cutting of the tunnel. Bending sections were redesigned to maintain the tunnel width while providing space for additional components (correctors, diagnostics) by adopting 2 T bending magnets with edge focusing and compact combined function quadrupole/sextupole magnets for chromatic corrections. The optics of the charge stripping area is optimized to better accommodate alternative stripping schemes. Segment 2 is now fully filled with cryomodules that were taken from Segment 3, to better optimize the layout for possible future energy upgrade. The RFQ output energy was increased to 0.5 MeV/u saving one cryomodule and 2 m of floor space. The final focusing system was optimized to better meet beam-on-target requirements, improve beam quality, and simplify operation. Two accelerating cryomodules were removed by taking advantage of higher performance cavities. Many other refinements, including optimization of the number of magnet types, etc., have taken place as well. The accelerator footprint and general layout has been frozen for over one year.

Front End

The FRIB Front End includes two ECR ion sources, two charge selection systems, a LEBT, RFQ, and MEBT [2]. To enhance availability and maintainability, the ECR sources and their charge selection systems are located at the ground level in the support building about 10 m above the linac tunnel floor, as shown in Fig. 2. The superconducting high-power source is based on the VENUS source developed at LBNL, and the room-temperature ARTEMIS source will be used primarily for commissioning. Both sources are placed on adjustable high voltage platforms to match the RFQ injection energy for different ion species.

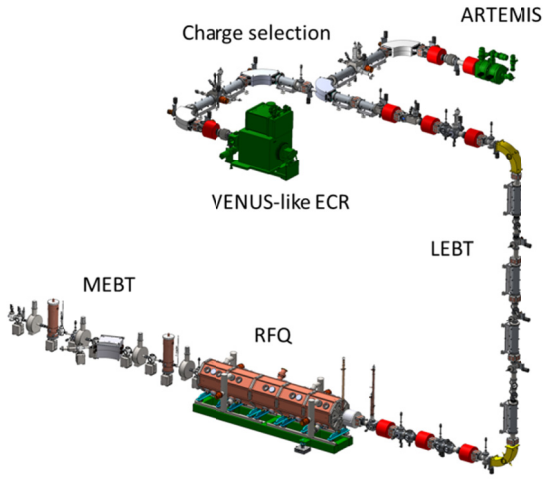

Figure 2: Layout of the Front End. Two ECR sources are located at the ground level. The RFQ and MEBT are located in the linac tunnel 10 m below grade.

The LEBT design is achromatic for transporting two charge states simultaneously. Beam collimation with apertures will be performed in the LEBT to improve the beam emittance injected into the downstream linac. The Front End will be able to vary beam intensity over several orders of magnitude as well as beam duty cycle and pulse length.

To achieve a small longitudinal output emittance from the RFQ, the cw beam from the ion source is pre-bunched in the LEBT by an external buncher (MHB) operating at 40.25, 80.5, and 120.75 MHz, simultaneously. The design philosophy of the unique single-gap gridless buncher is the same as the one built earlier for ReA3 [3]. For two-charge-state beam injection, following the MHB, a high-voltage platform together with a resonator conceptually similar to the MHB but operating only at 40.25 MHz is required. The adjustable HV platform is to make sure that the longitudinal separation of the two-charge-state beams equals one rf period of the RFQ at 80.5 MHz, while the resonator equalizes the energies of the two-charge-state beams at the entrance of the RFQ.

The RFQ beam physics design is based on an earlier design [4] and similar to the one under commissioning [5,6]. But the RFQ output energy was raised from 0.3 MeV/u to 0.5MeV/u by increasing its length to 5 m and implementing a linearly ramped inter-vane voltage that is nowadays widely used for a 4-vane structure. The RFQ output beam will be axial-symmetric to transversely match the downstream solenoid focusing channel. There are two rebunchers at the MEBT to better match into the superconducting linac longitudinally.

Superconducting Linac

One very unique feature of the FRIB arrangement is the acceleration and transportation of beam through three separate linacs within a single underground enclosure, a compact double-folded layout, to minimize the project construction costs. Segment 1 consists of two types of cryomodules with two different superconducting

ISBN 978-3-95450-118-2

resonators, which boost beam energy up to 20 MeV/u. The initial portion uses three cryomodules, each containing four β_{opt} = 0.041 QWRs and two superconducting solenoids. This is followed by 11 cryomodules of eight β_{opt} = 0.085 QWRs and three SC solenoids each. Both QWRs operate at 80.5 MHz. The beam apertures of the QWRs are increased from 30 to 34 mm without sacrificing much of rf performance. Table 1 lists beam dynamics related resonator parameters [7]. Each cavity is individually tunable for both voltage amplitude and phase. The strengths of the solenoids are up to 9 T. Alignment tolerance of these solenoids is ±1 mm under cryogenic conditions. Each solenoid has a pair of correctors (horizontal and vertical) and an associated cold BPM to facilitate orbit correction. Figure 3 shows a mechanical sketch of the two cryomodule types. Each warm region between cryomodules has a diagnostic box containing BPM, vacuum pump port, etc.

Table 1: Beam Dynamics Related Resonator Specifications

Type	β_{opt}	f (MHz)	Va (MV)	a (mm)
λ/4	0.041	80.5	0.81	34
λ/4	0.085	80.5	1.8	34
λ/2	0.29	322	2.1	40
λ/2	0.54	322	3.7	40

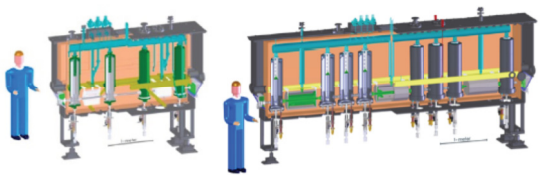

Figure 3: Illustrations of the β_{opt} = 0.041 (left) and β_{opt} = 0.085 (right) cryomodules used in Segment 1.

Segment 2 generates most of the energy gain through the linac. It also consists of two cavity types and corresponding cryomodules. The first portion is comprised of 12 cryomodules of half-wave resonators (HWRs) operating at 322 MHz with β_{opt} = 0.29. This is followed by 12 cryomodules of β_{opt} = 0.54 HWRs at the same frequency. Each of the HWR cryomodules contains a 0.5 m long solenoid with field up to 9 T. These two cryomodule types are illustrated in Fig. 4.

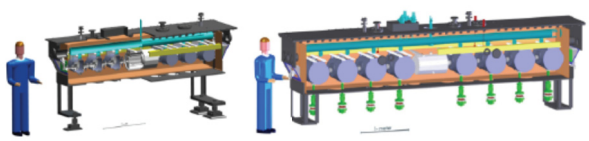

Figure 4: Illustrations of the β_{opt} = 0.29 (left) and β_{opt} = 0.54 (right) cryomodules used in Segment 2.

Six cryomodules of β_{opt} = 0.54 HWRs in Segment 3 complete the acceleration to >200 MeV/u followed by a transport section with sets of quadrupole doublets to the beam delivery system. The transport section would become filled with up to 12 additional cryomodules in the event of future energy upgrade.

Bending and Delivery Systems

The three accelerating segments are connected by two 180° bending systems. The first bending system begins with a charge stripper station occupying 2 m [8]. Quadrupoles are used, upstream and downstream of the station, to generate the desired spot size and large intrinsic angular spread at the stripper. A rebunching cryomodule upstream provides a minimum bunch length onto the stripper, while the downstream module reduces energy spread by increasing bunch length. Liquid lithium film is chosen as the primary stripping medium, which yields an average charge state of 78+ for uranium at ~17 MeV/u but with about 85% of particles in charge states 76+ through 80+ that can be selected and accelerated simultaneously. An alternative stripping process is to use helium gas cell, which produces a larger energy spread and slightly lower charge states than the lithium option. The FRIB lattice is designed to accommodate beam transport and acceleration of either option. To protect cryomodules from contaminants that could arise from the stripping process, two dog-leg systems, each consisting of four 5° rectangular dipoles, are located on either side of the stripper station to avoid line of sight. After the first 45° bending magnet, beam collimators, capable of sustaining full beam power of ~40 kW, are employed to select the charge states for further acceleration.

All the bending systems are achromatic transport, and combined function quadrupole/sextupole magnets are used between the bending magnets. The dipoles in the second 180° bending system will have superconducting coils with field up to 2 T. The bending systems also contain beam dumps primarily for beam tuning.

The 70° bending system with four 17.5° dipoles is used to guide the beam toward the fragmentation target. Just upstream of the target a quadrupole triplet is utilized to minimize chromatic aberrations and produce the desired final small beam spot.

BEAM DYNAMICS STUDIES

To evaluate the performance of the accelerator lattice under more realistic conditions, end-to-end beam dynamics simulations with high statistics have been performed using the code RIAPMTQ/IMPACT on high performance computers at MSU.

End-to-end Particle Tracking

Earlier beam studies of FRIB started with initial particles in water-bag distributions from the ion source. However, beams emanating from the ECR source often have complex phase space distributions. For a more realistic simulation, efforts were undertaken to mimic data taken from ion source measurements and then track through the linac. Figure 5 shows uranium data measured from the VENUS ion source at LBNL [9]. This distribution was then replicated for numerical input into the simulations of FRIB, as depicted in Figure 6 for both U^{33+} and U^{34+} with about half million particles each. The normalized rms emittance of the measured distribution is

ISBN 978-3-95450-118-2

~0.07 (π-mm-mrad), smaller than that used in previous simulations (0.1 π-mm-mrad), while the total emittances are slightly larger. However, when the "realistic" distribution is then tracked through the Front End, collimation is performed, resulting in similar total emittances of the two cases at the entrance of the RFQ. These particles were further tracked through Segment 1 and then five charge states (from U^{76+} through U^{80+}) were selected after the lithium stripper followed by two main acceleration segments. The final phase space distributions at the fragmentation target are shown in Figure 7. Beam-on-target requirements are met even for the most challenging multi-charge state uranium beam (e.g. >96 % of particles are within 1 mm diameter of beam spot size, all particles are within angular spread of ±5 mrad).

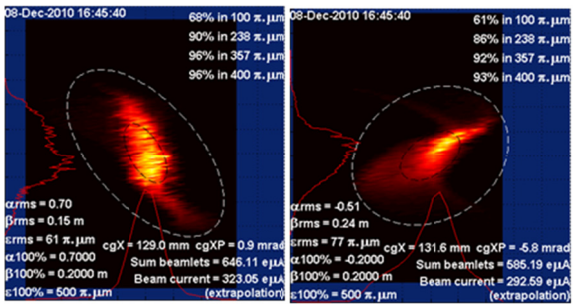

Figure 5: Measured horizontal (left) and vertical (right) phase space distributions for U^{33+} beam from VENUS.

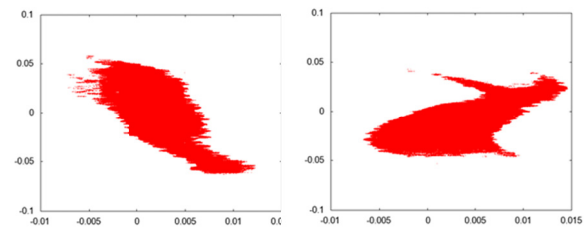

Figure 6: Generated horizontal (left) and vertical (right) phase space distributions for both U33+ and U34+ beam based on the measurement from VENUS in Fig. 4.

End-to-end simulation was also conducted for single charge argon beam identified as one of the primary beams for commissioning. As expected, results show the overall performance of argon is better than multi-charge uranium.

Beam simulation studies with machine errors were performed to evaluate the linac performance under more realistic conditions. Nominal machine errors used in the simulations are listed in Table 2, which seem reasonable and achievable. When the element displacements are introduced, especially the ±1 mm displacement of superconducting solenoids, correctors must be set properly for orbit correction based on the near BPMs, otherwise beam cannot be threaded through the linac.

A total of 200 random seeds combining the errors were used in the multi-charge-state uranium beam simulations. In each seed run, one million particles were tracked from the exit of RFQ through the three linac segments to the fragmentation target. Figure 8 illustrates the maximum beam envelope (in blue) at each longitudinal location of the 200 seeds together with the beam envelope without errors (in green) and linac radial apertures (in red). Beam evaluation results with machine errors show beam envelopes well within apertures. Beam envelope growth is mainly from misalignment (correctors were on). RF errors cause significant longitudinal emittance growth but is not coupled into transverse. No uncontrolled beam losses are observed with the nominal errors. Although errors impact the beam distributions on target, beam-on-target requirements are still met (>95% probability). The results are consistent with those of previous studies.

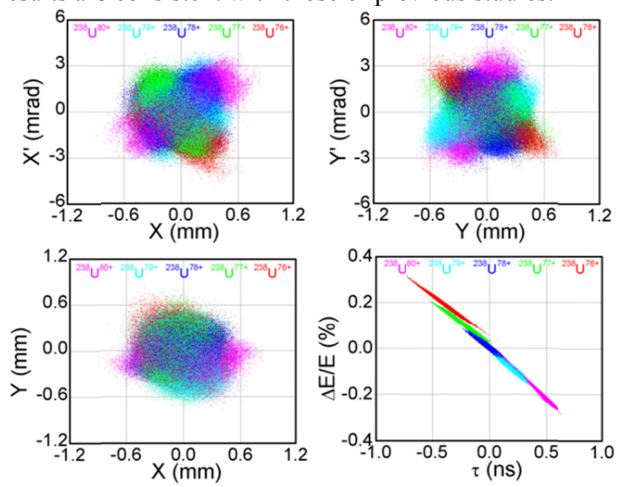

Figure 7: Transverse phase space plots (tops), physical beam size (bottom-left), and longitudinal phase space (bottom-right) distributions on target for 5-charge-state uranium without machine errors. The various colors represent the 5 different charge states.

Table 2: Nominal Machine Errors Used in Simulations

Name	Value	Distribution
Cold element displacement	±1 mm	Uniform
Warm element displacement	±0.4 mm	Uniform
Warm element rotation	±2 mrad	Uniform
BPM uncertainty	±0.4 mm	Uniform
Stripper thickness variation	±20%	Uniform
RF amplitude fluctuation	±1.5%	Gaussian(σ =0.5%)
RF phase fluctuation	±1.5°	Gaussian(σ =0.5°)

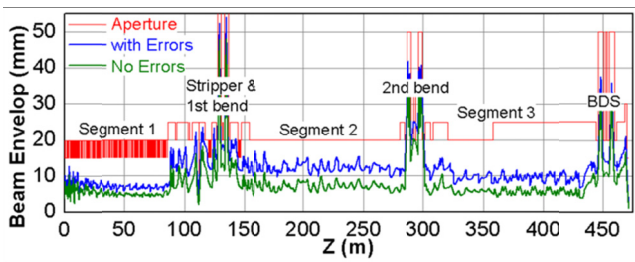

Figure 8: Beam envelopes along linac: beam element radial aperture in red, beam envelope without errors in green and with machine errors in blue.

To further evaluate the lattice sensitivity to errors, high statistics beam simulation was also studied using twice larger RF and placement errors than the nominal ones

ISBN 978-3-95450-118-2

listed in Table 2. In this case, beam losses occurred and the probability of beam loss of >1 W/m is ~14%. Naturally all beam loss occurs in the transverse direction, but the loss mainly initiated in low energy side due to the larger RF errors and distributed in Segment 2 and bending areas. Space is available for beam collimation/scraping in the warm transport sections (e.g., upstream of Segment 2). It has been found repeatedly that the sensitivity to dynamic cavity phase and amplitude errors are more important to overall performance, while magnet field errors and alignment errors are secondary.

Fault Conditions

During commissioning or operation, the performance of a cavity or cryomodule may not meet expectations, or a cavity or cryomodule may be unexpectedly out of specifications. While there are obviously many individual instances that could be studied, a few typical cases and obvious situations are explored. As an example, we suppose that the cavity gradients in all of the QWRs are lower than the design by 20%. In this case, the average charge state after the lithium stripper drops to 76+ from 78+ for uranium beams. The linac output energy becomes about 190 MeV/u instead of 202 MeV/u. On the other hand, if the HWR gradients are systematically lower by 20%, then the linac output energy is reduced to ~150 MeV/u. To recover the beam energy on target, six additional β_{opt} = 0.54 cryomodules would be required. Studies also show single element (cavity, solenoid) or cryomodule failure appears manageable either by tuning adjacent elements or replacing with a spare. Systematic studies of failure modes and recovery continue.

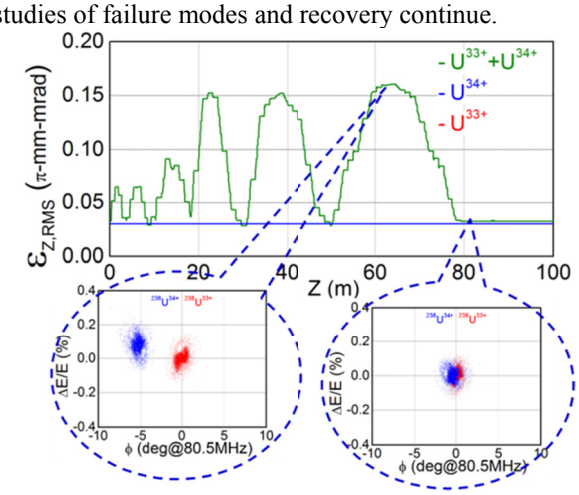

Figure 9: Longitudinal emittance of two-charge-state uranium beam along Segment 1 together with sampled particles (33+ red, 34+ blue) in longitudinal phase space.

Beam Tuning

To protect the machine from damage, beam with low current, short pulse, and reduced rep rate will be used during machine setup and tuning to decrease beam power. Beam current will be as low as 50 euA. Pulse duration will be as short as 50 us. And rep rate will be as low as possible (1 Hz, even single shot). Beam tuning will be started with a single-charge-state reference beam controlled by the charge state selection slits, and then optimized with other charge state(s). Model-based on-line tuning is proposed not only to reduce tuning and recovery time, but also to provide a platform and perform global optimization. Cavity synchronous phase setup, orbit correction, and Twiss parameters matching are simulated. It is required to overlap the two-charge-state beam transversely and longitudinally at stripper to minimize the emittance growth due to stripping. Due to the different longitudinal motion, the two charge states oscillate from each other, as shown in Fig. 9. The phases of cavities in Segment 1 are adjusted so as to longitudinally overlap the two-charge-state beam at the exit of Segment 1 by measuring the timing of each charge state beam.

CONCLUSION

The FRIB driver linac lattice has been optimized and finalized, consistent with the proposed baseline requirements and future upgrades. The accelerator layout footprint has been frozen since June 2011. The verified linac lattice is compatible with the civil engineering final design. This accelerator design is documented in the FRIB Lattice File, Parameter List, engineering drawings, and requirements documents.

End-to-end beam simulations with errors have been performed and various fault conditions explored. Results indicate that beam-on-target requirements can be met under realistic conditions, while maintaining uncontrolled beam loss to < 1 W/m, and the lattice design is robust. Linac beam tuning strategies and algorithms are studied, and virtual accelerator and on-line control mode are being developed to support commissioning and operations.

ACKNOWLEDGMENT

We thank the contributions of our colleagues at MSU: N. Bultman, P. Chu, J. Crisp, C. Compton, P. Gibson, P. Guetschow, K. Holland, M. Johnson, D. Leitner, M. Leitner, G. Morgan, D. Morris, S. Peng, J. Popielarski, X. Rao, T. Russo, K. Saito, M. Shupter, R. Webber, A. Zeller, Z. Zheng and many others. We also thank A. Aleksandrov, J. Bisognano, H. Edwards, J. Galambos, S. Henderson, G. Hoffstaetter, N. Holtkamp, B. Laxdal, P. Ostroumov, S. Ozaki, R. Pardo, S. Peggs, J. Qiang, D. Raparia, T. Roser, J. Stovall, L. Young, etc. for their valuable advice, discussions, and collaborations.

REFERENCES

[1] J. Wei, et al., HIAT'12, MOB01 (2012, in press).
[2] E. Pozdeyev, et al., LINAC'12, (2012, in press).
[3] Q. Zhao, et al, LINAC'08, Victoria, BC, p. 948.
[4] Q. Zhao, et al, LINAC'04, Lübeck, Germany, p. 599.
[5] Q. Zhao, et al, PAC'07, Albuquerque, NM, p.1772.
[6] D. Leitner, et al, PAC'11, New York, NY, p. 1912.
[7] A. Facco, et al, IPAC'12 (2012, in press).
[8] F. Marti, et al., LINAC'12, (2012, in press).
[9] G. Machicoane, et al., ECRIS'12, (2012, in press).
[10] Q. Zhao, et al., PAC'09, Vancouver, BC, p. 3901.

ISBN 978-3-95450-118-2